Immunodeficiencies and autoimmunity

Clinical

Research Article

Clonally expanded PD-1-expressing T cells are enriched in synovial fluid of juvenile idiopathic arthritis patients

Anna Vanni[#1], Alessio Mazzoni[#1,2], Roberto Semeraro[#1], Manuela Capone[1], Patrick Maschmeyer[3,4,5], Giulia Lamacchia[1], Lorenzo Salvati[1], Alberto Carnasciali[1], Parham Farahvachi[1], Teresa Giani[6], Gabriele Simonini[6], Giovanni Filocamo[7], Micol Romano[8], Francesco Liotta[1,9], Mir-Farzin Mashreghi[10], Lorenzo Cosmi[1,11], Rolando Cimaz[12], Alberto Magi[13], Laura Maggi[1] and Francesco Annunziato[1,2]

[1] Department of Experimental and Clinical Medicine, University of Florence, Florence, Tuscany, Italy
[2] Flow Cytometry Diagnostic Center and Immunotherapy, Careggi University Hospital, Florence, Tuscany, Italy
[3] Institute of Health (BIH) at Charité, Universitätsmedizin Berlin, Berlin, Berlin, Germany
[4] Max-Delbrück-Center for Molecular Medicine in the Helmholtz Association (MDC), Institute for Medical Systems Biology (BIMSB), Berlin, Berlin, Germany
[5] Department of Hematology, Oncology and Cancer Immunology, Charité-Universitätsmedizin Berlin, Berlin, Berlin, Germany
[6] AOU Meyer, Florence, Tuscany, Italy
[7] Pediatric Rheumatology, Fondazione IRCCS Cà Granda Ospedale Maggiore Policlinico, Milano IT and University of Milan, Milan, Lombardy, Italy
[8] University of Western Ontario, London, Ontario, Canada
[9] Immunology and Cell Therapy Unit, Careggi University Hospital, Florence, Tuscany, Italy
[10] Deutsches Rheuma-Forschungszentrum (DRFZ), Institute of the Leibniz Association, Berlin, Berlin, Germany
[11] Immunoallergology Unit, Careggi University Hospital, Florence, Tuscany, Italy
[12] Department of Clinical Sciences and Community Health, Research Center for Adult and Pediatric Rheumatic Diseases, University of Milan, Milan, Lombardy, Italy
[13] Department of Information Engineering, University of Florence, Florence, Tuscany, Italy

Juvenile idiopathic arthritis (JIA) is the most common chronic rheumatic condition in childhood. The disease etiology remains largely unknown; however, a key role in JIA pathogenesis is surely mediated by T cells. T-lymphocytes activity is controlled via signals, known as immune checkpoints. Delivering an inhibitory signal or blocking a stimulatory signal to achieve immune suppression is critical in autoimmune diseases. However, the role of immune checkpoints in chronic inflammation and autoimmunity must still be deciphered. In this study, we investigated at the single-cell level the feature of T cells in JIA chronic inflammation, both at the transcriptome level via single-cell RNA sequencing and at the protein level by flow cytometry. We found that despite the heterogeneity in the composition of synovial CD4+ and CD8+ T cells, those characterized by PD-1 expression were clonally expanded tissue-resident memory (Trm)-like cells and displayed the highest proinflammatory capacity, suggesting their active contribution in sustaining chronic inflammation in situ. Our data support the concept that novel therapeutic strategies targeting PD-1 may be effective in the treatment of JIA. With this approach, it may become possible to target overactive T cells regardless of their cytokine production profile.

🖥 Additional supporting information may be found online in the Supporting Information section at the end of the article.

Correspondence: Dr. Laura Maggi and Prof. Francesco Annunziato
e-mail: laura.maggi@unifi.it; francesco.annunziato@unifi.it

#Anna Vanni, Alessio Mazzoni, and Roberto Semeraro contributed equally to this work.

Introduction

Juvenile idiopathic arthritis (JIA) is a heterogeneous group of chronic inflammatory arthritides of unknown etiology affecting children under 16 years of age and causing short- and long-term disability [1–3]. Previous studies suggested a central role of T cells in JIA pathogenesis [4, 5]. Indeed, CD4+ and CD8+ T cells with an activated phenotype are elevated within affected joints [6]. It has been shown that alterations in T-cell co-stimulatory and co-inhibitory immune checkpoint (IC) molecules, responsible for regulating the immune response, lead to the development of chronic inflammatory and autoimmune diseases [7, 8]. The expression of high levels of IC with inhibitory function on activated T cells is a physiological phenomenon crucial to avoid an excessive response, which can result in tissue damage. Indeed, these pathways lead to exhaustion and functional inactivation of T cells and, accordingly, T cells expressing IC, especially PD-1 and CTLA-4, which are enriched in tumor infiltrates. Monoclonal antibodies inhibiting PD-1 or CTLA-4, thus, reactivate latent antitumoral immunity, and are currently approved for many neoplastic diseases. In contrast, only a few studies have evaluated the role of ICs in inflammatory diseases [9]. Chronic inflammatory diseases are typically sustained by overactive T cells, thus, understanding how their functionality can be regulated is of primary importance. Indeed, the identity and dynamics of T cells as well as their functional differentiation stage at sites of inflammation are still largely unexplored, and an in-depth analysis of these aspects can pave the way for new therapeutic approaches.

In the present study, we performed a detailed characterization at the single-cell level of T cells in children with JIA. We found that although IC expression is increased on synovial fluid (SF) T cells of JIA patients, PD-1-expressing lymphocytes retain their effector capacity, producing high levels of proinflammatory cytokines. Our results also point out that these effector T cells express markers of tissue residency, suggesting their active contribution in sustaining chronic inflammation in situ.

Results

SF of JIA patients is enriched in CD4+ T cells expressing TIGIT and PD1

To identify subsets of T cells sustaining chronic inflammation in JIA, we reanalyzed publicly available single-cell RNA-sequencing (scRNA-seq) data of memory CD4+ and CD8+ T cells derived from six SF and six peripheral blood (PB) samples of oligoarticular JIA patients [10] (GSE160097). Total CD4+ T cells from all patients were characterized separately from CD8+ T cells.

To proceed with our analysis, we first evaluated the scRNA-seq dataset composition to confirm Maschmeyer et al.'s observations [10]. Visualizing data through the uniform manifold approximation and projection (UMAP) algorithm and coloring cells based on their tissue origin, we observed that CD4+ T cells from both PB and SF grouped separately, as for the author dataset (Support-

ing Information Fig. S1A). Next, we clustered the data, obtaining seven groups (Supporting Information Fig. S1B and C), and confirmed their nature by looking for the expression of canonical markers from key immune cell types, states and pathways, already used by Julé et al. [11] (Supporting Information Fig. S1D) and genesets adopted by Maschmeyer et al. (Supporting Information Fig. S1G and H). We identified three clusters dominated by cells with a T-central memory (Tcm) profile (*SELL, CCR7,* and *TCF7*) deriving mainly from PB, two clusters with a T-effector signature, one cluster with tissue-resident memory (Trm) features, and one cytotoxic (Supporting Information Fig. S1B–D). Among Tcm clusters, one showed an enrichment of Th17-associate genes, such as *KLRB1, CCR6, RORC, and CTSH* (Tcm-TH17-like) (Supporting Information Fig. S1D–F), while another showed upregulation of IFN-induced genes (IFN stimulated). Notably, some cells of the IFN-stimulated cluster expressed a gene set typical of cycling T cells (REACTOME_CELL_CYCLE) (Supporting Information Fig. S1G and H). On the other hand, the remaining four clusters contained the majority of SF cells. In particular, the Trm cluster showed a Trm gene signature and an enrichment of genes indicating TCR stimulation (Supporting Information Fig. S1G and H). In addition, we observed that Cytotoxic CD4+ T-cell cluster expressed high levels of the cytotoxic markers *GZMA* and *PRF1*, along with the activation marker *HLA-DRB1*, and low levels of ribosomal genes (Supporting Information Fig. S1E). Interestingly, both Trm and cytotoxic CD4+ T clusters expressed high levels of the IC *PDCD1* (Supporting Information Fig. S1D). *PDCD1* was also expressed by the Teff-TIGIT+ cluster, which was also characterized by the expression of additional IC such as *TIGIT* and *CTLA-4*. The high expression of IC markers suggests chronic reactivation of these lymphocytes in vivo. Finally, Trm and Teff-TIGIT+ cells contained cells resembling both Th1 (*CXCR3, TBX21, IFNG*) and Th17 (*KLRB1, CCR6, RORC*) signatures, suggesting a bona fide Th17-derived (nonclassic) Th1 phenotype (Supporting Information Fig. S1D and F). These results confirmed the notion of a prevalence of Th1- and Th17-like CD4+ T cells in the SF of JIA patients [12–14].

To evaluate the relationships between these populations and define their differentiation processes, we performed a trajectory analysis using the tool Slingshot. The lineage inference identified a trajectory that originated from the PB cluster Tcm, passed through the PB Tcm clusters IFN-stimulated and Tcm–TH17-like, and then bifurcated on SF cluster Teff-KLRB1+. The resulting two branches terminated their paths on SF clusters Teff-TIGIT+ and Trm respectively, both characterized by an enrichment of effector- and resident-memory-like genes (Fig. 1A–C). Interestingly, terminal clusters Teff-TIGIT+ and Trm differed for cytotoxicity marker expression; indeed, we observed a decline in cytotoxic gene levels through branch 1, while they increased along branch 2 (Fig. 1B and C). Moreover, as observed before, both terminal clusters showed high levels of ICs *PDCD1* and *TIGIT*. In particular, we observed an increased expression of *TIGIT* alone or co-expressed with *PDCD1* in terminal cluster Teff-TIGIT+. On the contrary, branch 2 was mainly characterized by *PDCD1* expression, reaching the highest levels in terminal clusters Cytotoxic CD4+ T and Trm (Fig. 1B and D). Importantly, both terminal
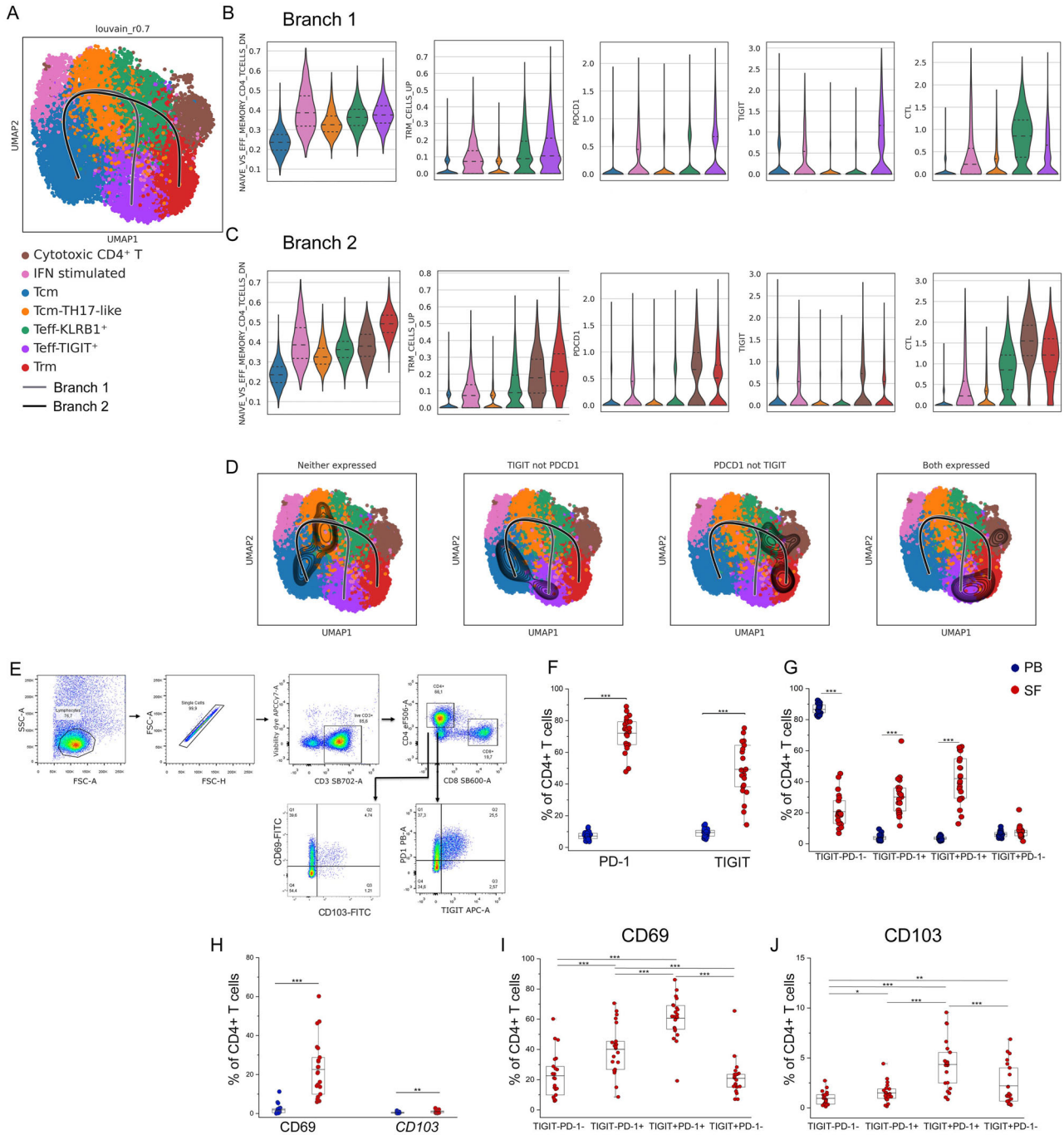
Figure 1. Increased expression of inhibitory checkpoint molecules by SF-infiltrating CD4$^+$ T cells. (A) Slingshot trajectory obtained from scRNA-seq data of pooled CD4$^+$CD45RO$^+$ cells obtained from PB and SF of six patients impressed over identified clusters. (B and C) Modules score of gene sets (NAÏVE_VS_EFF_MEMORY_CD4_TCELLS_DN and TRM_CELLS_UP) and of PDCD1, TIGIT and CTL genes are reported for each cluster as Violin plot. Clusters are divided based on the trajectory lineage: (B) Branch 1 and (C) Branch 2. (D) UMAP visualization of pseudotime trajectory together with the differential expression of ICs markers TIGIT and PDCD1, reported as density lines. (E) Representative example (out of 22 experiments) showing gating strategy of CD4$^+$ T cells expressing PD-1 and TIGIT in PB and SF. Lymphocytes were gated based on physical parameters (FSC-SSC), then doublets were removed using FSC-A and FSC-H parameters. Dead cells were excluded using viability stain and T cells were identified as CD3$^+$. We then identified CD4$^+$ cells on which we evaluated TIGIT, PD-1, CD69, and CD103 expression. (F) Expression of PD-1 and TIGIT on total CD4$^+$ T cells obtained from PB (n = 22) and SF (n = 22). (G) Frequency of CD4$^+$ T cells in TIGIT$^-$PD-1$^-$, TIGIT$^-$PD-1$^+$, TIGIT$^+$PD-1$^+$, TIGIT$^+$PD-1$^-$ subsets. (H) Evaluation of CD69 and CD103 expression on total CD4$^+$ T cells (n = 22) and in TIGIT$^-$PD-1$^-$, TIGIT$^-$PD-1$^+$, TIGIT$^+$PD-1$^+$, TIGIT$^+$PD-1$^-$ subsets (I, J). Flow cytometric data (F-J) are obtained from 22 independent experiments. Red dots represent SF cells and blue dots represent PB lymphocytes from individual donors. Boxes indicate mean values and 25th and 75th percentiles. Whiskers indicate minimum and maximum values. Statistical analysis was performed by Wilcoxon-Signed Rank test (*$p < 0.05$, **$p < 0.01$, ***$p < 0.001$).

clusters Teff-TIGIT$^+$ and Trm showed a typical activated and effector gene signature, which is in contrast with the presence of high levels of ICs usually associated with an exhausted phenotype.

To gain more insights on this phenomenon, we also investigated by flow cytometry the expression of the two distinctive ICs, PD-1 and TIGIT. Using the gating strategy shown in Fig. 1E, we observed that CD4$^+$ T cells from SF displayed significantly higher expression of both PD-1 and TIGIT, when compared to PB (Fig. 1F and H). The combinatorial expression of the two ICs defined four distinct subsets: TIGIT$^-$PD-1$^-$, TIGIT$^-$PD-1$^+$, TIGIT$^+$PD-1$^+$, TIGIT$^+$PD-1$^-$. CD4$^+$ T cells with a TIGIT$^-$PD-1$^-$ phenotype were preferentially enriched in PB as opposed to SF. On the contrary, TIGIT$^-$PD-1$^+$ and TIGIT$^+$PD-1$^+$ cells were present at higher frequencies in SF. TIGIT$^+$PD-1$^-$ cells were poorly represented and showed comparable frequencies in PB and SF (Fig. 1G).

Since scRNA-seq data showed that CD4$^+$ T cells from SF can also express typical genes of tissue residency (Fig. 1B and C), we evaluated at the protein level the expression of CD69 and CD103, markers of tissue residency. CD4$^+$ T cells from SF showed a significantly higher expression of both CD69 and CD103 compared to PB (Fig. 1H). Remarkably, T cells with a TIGIT$^+$PD-1$^+$ phenotype expressed the highest levels of both CD69 and CD103, followed by the TIGIT$^-$PD-1$^+$ population. The TIGIT$^-$PD-1$^-$ and the TIGIT$^+$PD-1$^-$ subsets instead exhibited the lowest percentage of cells expressing Trm markers (Fig. 1I and J).

Phenotypic and functional characterization of SF CD4$^+$ T cells

We assessed the functional properties of the different CD4$^+$ T-cell subsets by measuring the production of several cytokines (IL-2, IFN-γ, TNF-α, GM-CSF, IL-17, IL-10) directly ex vivo via scRNA-seq or following restimulation by flow cytometry.

Cytokine expression projected on pseudotime trajectory and dot plot showed that *IFNG and TNF* were mainly expressed by T cells from SF (Fig. 2A and B). In particular, cells of terminal cluster Trm expressed both *TNF* and *IFNG*, while cells of terminal cluster Teff-TIGIT$^+$ expressed a lower amount of proinflammatory cytokines (Fig. 2B). Consistent with data observed at the single-cell transcriptomic level, flow cytometric data showed that SF CD4$^+$ T cells produced significantly more IFN-γ, TNF-α, GM-CSF, and IL-10 compared to PB (Fig. 2C). On the contrary, no differences were observed in terms of IL-2 and IL-17 production.

Focusing on cytokine production by the four subsets identified based on TIGIT and PD-1 expression (Fig. 2D–I), we observed that SF CD4$^+$ T cell subsets produced higher levels of IFN-γ, TNF-α, GM-CSF compared to the corresponding PB populations, while IL-2, IL-17, and IL-10 production was comparable. Focusing on SF CD4$^+$ T cells, we found that IFN-γ, TNF-α, GM-CSF, and IL-2 were significantly more expressed by the TIGIT$^-$PD-1$^+$ subset, followed by the TIGIT$^-$PD-1$^-$ and TIGIT$^+$PD-1$^+$ populations. The TIGIT$^+$PD-1$^-$ population instead exhibited the lowest percentage of cells producing these cytokines. Regarding IL-10, it was mainly produced by TIGIT$^-$PD-1$^+$ and TIGIT$^+$PD-1$^+$ cells,

although at significantly lower frequency than proinflammatory cytokines. The same hierarchy could be observed also in the four CD4$^+$ T-cell subsets from PB, with the exception of the TIGIT$^-$PD-1$^-$ subset, which produced the lowest percentage of all analyzed cytokines, differently from what we observed in SF.

TCR repertoire analyses reveal clonal relationship of synovial CD4$^+$ T cells

To gain insight into the clonal relationship among individual CD4$^+$ T cells, we reconstructed their TCR sequences from scRNA-seq data. The majority of clonotypes were private singletons (Supporting Information Fig. S2A) and only 2–7% of patient PB clonotypes were clonally expanded contrary to the 12–19% deriving from SF (Fig. 3A). Interestingly, among the seven identified clusters, the Trm cluster showed the highest proportion of clonally expanded cells (Fig. 3B) and, consistent with this observation, had the lowest alpha diversity of clone types, suggesting a positive selection for certain, reactive T-cell clones (Supporting Information Fig. S2B). This observation was supported also by the trajectory analysis, which showed an enrichment of expanded clones at the end of branch 2, which terminates on the Trm cluster (Fig. 3C). Analyzing more in detail the clonal expansion in the two branches of the trajectory, we observed an increase of clonal expansion along the pseudotime in both branches (Fig. 3D and E). To understand if the two trajectories identified by trajectory analysis represent mutually exclusive lineages or alternatively can evolve one in the other, we evaluated the distribution of TCRs in the seven identified clusters. Notably, as shown in Fig. 3F, the most expanded clones (i.e. 3842 and 4663) were shared between trajectory terminal clusters Trm and Teff-TIGIT$^+$. These observations suggest that CD4$^+$ cells of different clusters might undergo state transitions upon proper microenvironmental stimulation.

Phenotypical and functional characterization of SF CD8$^+$ T cells

The same approach was used to dissect the diversity of CD8$^+$ T cells. Also in this case, UMAP visualization colored by tissue origin showed that CD8$^+$ T cells from PB and SF grouped separately, with few exceptions (Supporting Information Fig. S3A). Next, we clustered the data, obtaining eight groups (Supporting Information Fig. S3B and C), and confirmed their nature as for CD4$^+$ T cells. In particular, we identified two Tcm clusters, three Teff clusters, a Trm population, along with an IFN-stimulated cluster and an interesting cluster defined as NKT-KLRB1 (Supporting Information Fig. S3B–D).

Looking at the UMAP visualization, we observed that the NKT-KLRB1 cluster segregates separately from other CD8$^+$ T cells. Interestingly, these cells expressed high levels *of KLRB1, CCR6, RORC, IL7R, IL23R, IL17RE* and cytotoxic genes such as *PRF1, GZMA*, and low levels of *CD8B* gene (Supporting Information Figs. S3D and S4), resembling a gene signature already described and
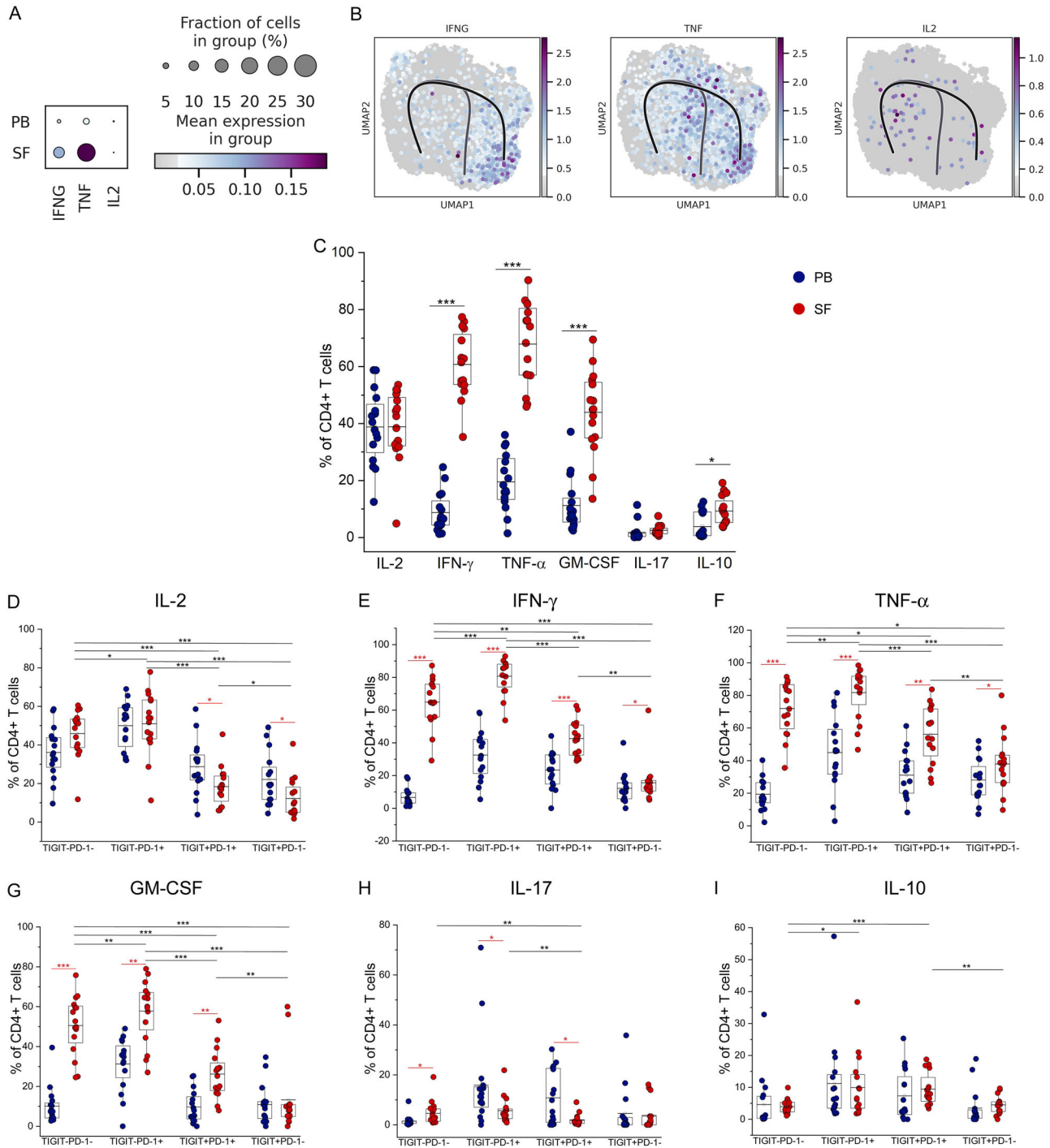
Figure 2. Functional characterization of PB and SF CD4$^+$ T-cell subsets expressing distinct combinations of inhibitory checkpoints. (A) Dot plot representation of scRNA-seq data showing the mean expression of cytokine genes in pooled CD4$^+$CD45RO$^+$ T cells from PB and SF of six patients. The size of the dot is proportional to the percentage of cells expressing the gene in that cluster, and the color code illustrates the average level of expression of all cells in the cluster. (B) UMAP visualization of CD4 cells colored by cytokines expression levels. (C) Frequency of total CD4$^+$ T cells producing cytokines (IL-2, IFN-γ, TNF-α, GM-CSF, IL-17, IL-10). Frequency of CD4$^+$ T cells subsets (TIGIT$^-$PD-1$^-$, TIGIT$^-$PD-1$^+$, TIGIT$^+$PD-1$^+$, TIGIT$^+$PD-1$^-$) producing IL-2 (D), IFN-γ (E), TNF-α (F), GM-CSF (G), IL-17 (H), IL-10 (I). (C-I) T cells were obtained from PB (blue dots) (n = 16) and SF (red dots) (n = 16) samples. Flow cytometric data (C-I) are obtained from 16 independent experiments. Boxes indicate mean values and 25th and 75th percentiles. Whiskers indicate minimum and maximum values. Statistical analysis was performed by Wilcoxon-Signed Rank test (*$p < 0.05$, **$p < 0.01$, ***$p < 0.001$). Red asterisks refer to paired statistics of PB compared to SF samples. Black asterisks represent paired statistics within each TIGIT and PD-1 subsets in SF samples.
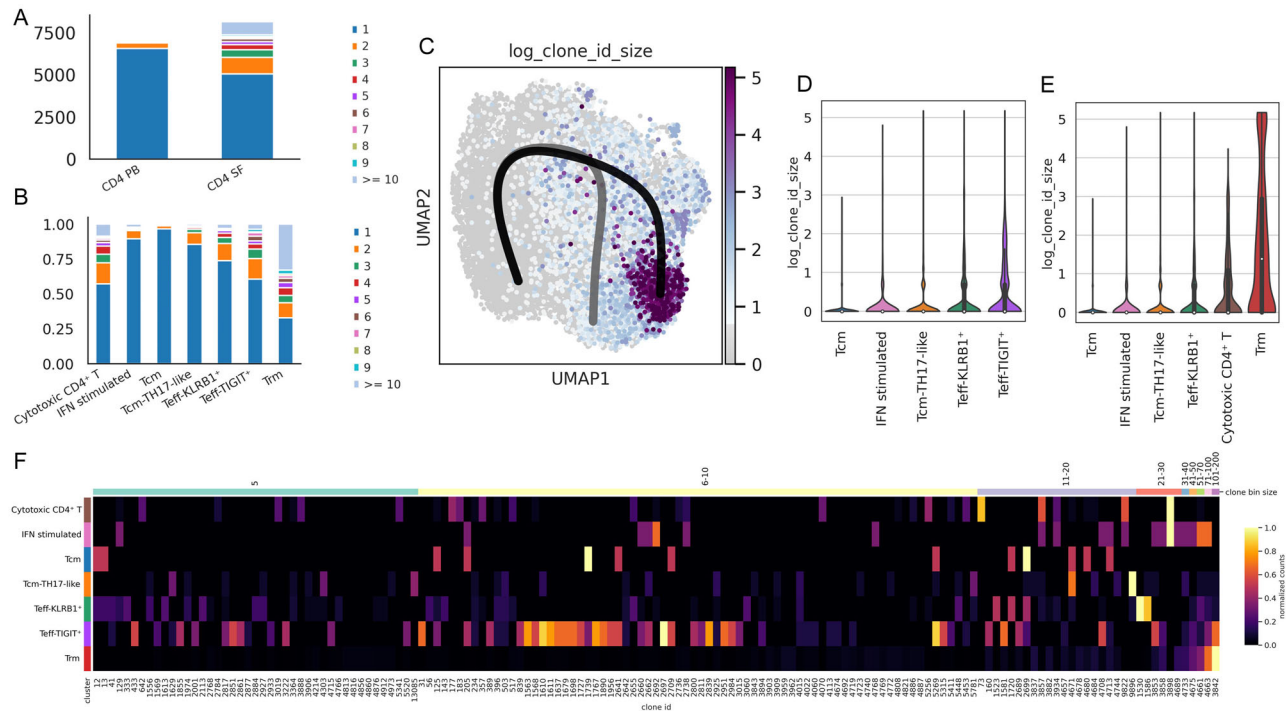
Figure 3. Single-cell TCR profiling of PB and SF CD4$^+$ T lymphocytes. Bar plots showing the clonal expansion of CD4$^+$ T cells from PB and SF of six patients (A) divided based on tissue origin or (B) divided in the identified clusters, each color represents the number of cells within the same TCR. (C) UMAP visualization of pseudotime trajectory together with clone size score in a logarithmic scale. Visualization of clone size as Violin plot in branch 1 (D) and branch 2 (E) clusters. (F) Heatmap showing the presence or absence of a specific clone in all identified cluster, the color code illustrates the relative abundance of each clone in the corresponding cluster. Clones are grouped by clone size and only clones with ≥ 5 cells were shown.

attributed to NKT cells [15, 16] and a particular subset of innate-like CD8$^+$ T cells [17]. The two Tcm clusters, enriched in cells with Tcm profile (*SELL, CCR7,* and *TCF7*), differed for CXCR3 gene expression, thus, were defined as Tcm and Tcm-CXCR3$^+$, respectively. Interestingly, these clusters showed very low levels of cytotoxicity markers compared with other PB clusters (Supporting Information Fig. S4D–F). One Teff cluster (Teff-GNLY$^+$) showed high levels of effector markers compared to the other PB cells, and in particular, expressed high levels of the cytotoxic molecules and the gene *GNLY*. Another Teff cluster (CD8 TIGIT$^+$) composed both by PB and SF cells, comprised cells with high levels of *TIGIT* expression. Interestingly, the majority of SF cells were contained in two clusters: the Trm cluster with a Trm signature and the CD8-Teff cluster, showing high levels of cytotoxic markers *GZMA* and *PRF1* along with activation marker *HLA-DRB1*, the ICs *PDCD1, TIGIT, LAG3* (Supporting Information Fig. S3D–F) and low levels of ribosomal genes (Supporting Information Fig. S3C). In addition, we observed the IFN-stimulated cluster comprising all CD8$^+$ cycling cells both from PB and SF samples (Supporting Information Fig. S3D–F).

Next, as for CD4$^+$ cells, we performed a trajectory analysis to define the cell differentiation stages of CD8$^+$ T cells (Fig. 4A). The Slingshot algorithm identified a trajectory that originated from the Tcm-CXCR3$^+$ cluster (composed both by PB and SF cells) and branched out in four directions, terminating on two PB clusters

(NKT-KLRB1 and Teff-GNLY$^+$) and two SF clusters (Trm and CD8-Teff). Branch 1 terminated on the NKT-KLRB1 cluster, containing cells resembling NKT or innate CD8$^+$ T-cell signatures (Fig. 4B), on the other hand, branch 2 ended on the Teff-GNLY$^+$ cluster, which expressed high levels of cytotoxicity markers, along with NKT-KLRB1 cluster (Fig. 4C).

Branches 3 and 4 instead terminated their paths on SF clusters CD8-Teff and Trm, respectively, both characterized by an enrichment of resident-memory-like genes (Fig. 4D and E). As for CD4$^+$ T cells, also in this case, we retrieved *PDCD1* and *TIGIT* expression in terminal SF clusters, while there was no expression in the terminal PB ones. In particular, the CD8-Teff terminal cluster, contained the majority of cells expressing higher levels of both *PDCD1* and *TIGIT*, resembling the terminal cluster Teff-TIGIT$^+$ of CD4$^+$ cells (Fig. 4B–F). Interestingly, the CD8-Teff cluster, together with high levels of ICs, expressed also the highest level of the exhaustion markers *TOX* (Supporting Information Fig. S5).

For these reasons, we investigated by flow cytometry the expression of TIGIT and PD-1 molecules by CD8$^+$ T cells obtained from PB and SF samples (see Fig. 4G for gating strategy). CD8$^+$ T cells showed a significantly higher expression of both TIGIT and PD-1 in SF compared to PB (Fig. 4H). The combinatorial expression of the two ICs defined four populations: TIGIT$^-$PD-1$^-$, TIGIT$^-$PD-1$^+$, TIGIT$^+$PD-1$^+$, and TIGIT$^+$PD-1$^-$. However, as already observed by scRNA-seq analysis, we also confirmed at pro-
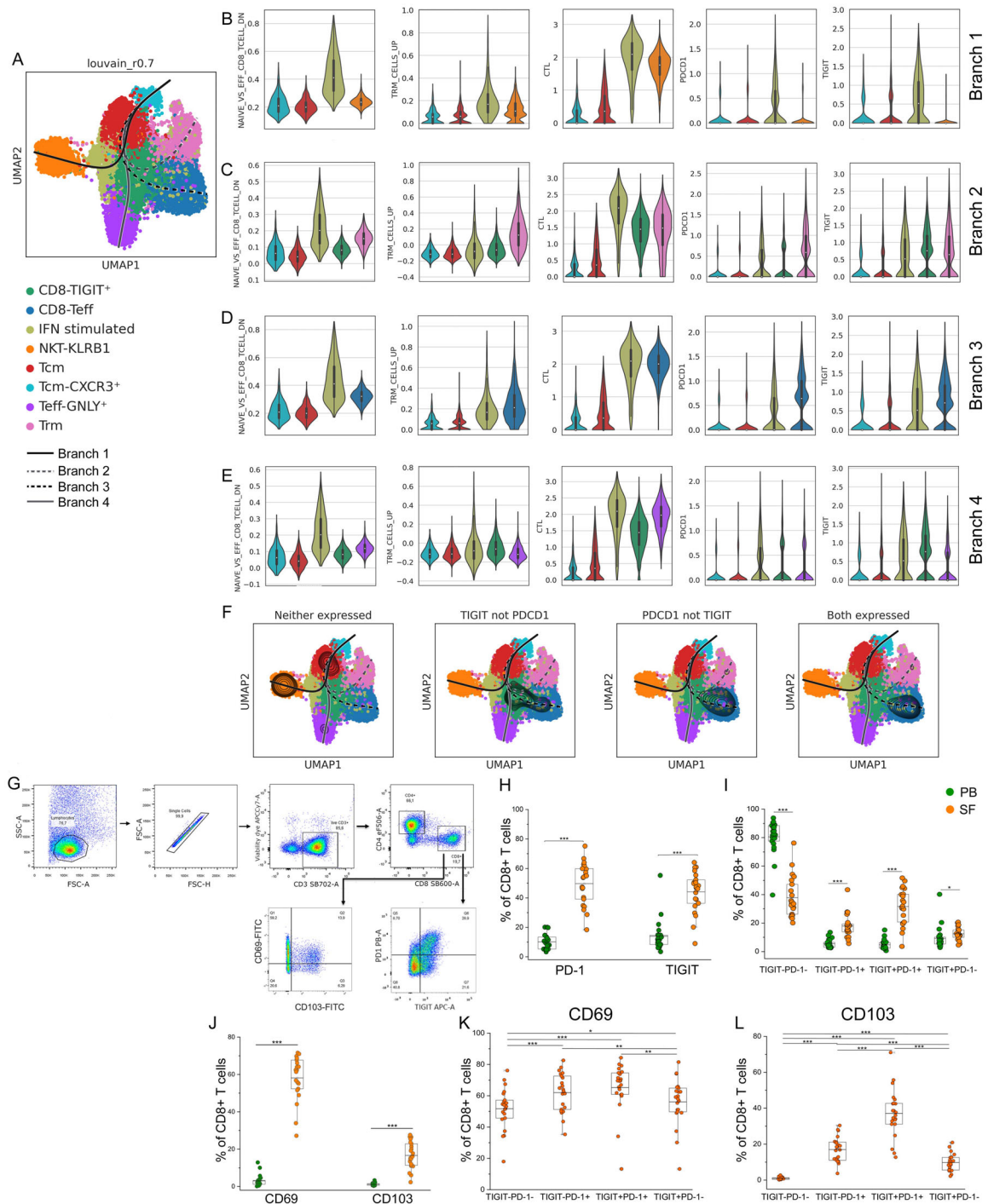
Figure 4. Increased expression of inhibitory checkpoint molecules by SF-infiltrating CD8$^+$ T cells. (A) Slingshot trajectory obtained from scRNA-seq data of pooled CD8$^+$CD45RO$^+$ cells obtained from PB and SF of six patients impressed over identified clusters. (B-D) Modules score of gene sets (NAÏVE_VS_EFF_MEMORY_CD4_TCELLS_DN and TRM_CELLS_UP) and of PDCD1, TIGIT and CTL genes are reported for each cluster as violin plot. Clusters are divided based on the trajectory lineage: (B) branch 1, (C) branch 2, (D) branch 3, and (E) branch 4. (F) UMAP visualization of pseudotime trajectory together with the differential expression of ICs markers TIGIT and PDCD1, reported as density lines. (G) Representative example (out of 22 experiments) showing gating strategy of CD8$^+$ T cells expressing PD-1 and TIGIT in PB and SF. Lymphocytes were gated based on physical parameters (FSC-SSC), then doublets were removed using FSC-A and FSC-H parameters. Dead cells were excluded using viability stain and T cells were identified as CD3$^+$. We then identified CD8$^+$ cells on which we evaluated TIGIT, PD-1, CD69, and CD103 expression. (H) Expression of PD-1 and TIGIT on total CD8$^+$ T cells obtained from PB (n = 22) and SF (n = 22). (I) Frequency of CD8$^+$ T cells in TIGIT$^-$PD-1$^-$, TIGIT$^-$PD-1$^+$, TIGIT$^+$PD-1$^+$, TIGIT$^+$PD-1$^-$ subsets. (J) Evaluation of CD69 and CD103 expression on total CD8$^+$ T cells and in TIGIT$^-$PD-1$^-$, TIGIT$^-$PD-1$^+$, TIGIT$^+$PD-1$^+$, TIGIT$^+$PD-1$^-$ subsets (K,M). Green dots represent SF cells and orange dots represent PB lymphocytes from individual donors. Flow cytometric data (H-M) are obtained from 22 independent experiments. Boxes indicate mean values and 25th and 75th percentiles. Whiskers indicate minimum and maximum values. Statistical analysis was performed by Wilcoxon-Signed Rank test (*$p < 0.05$, **$p < 0.01$, ***$p < 0.001$).

tein level that CD8$^+$ T cells expressing PD-1 but lacking TIGIT are very rare. Similarly to CD4$^+$ T cells, TIGIT$^-$PD-1$^-$ CD8$^+$ T cells were enriched in PB compared to SF, while CD8$^+$ T cells expressing at least one IC (TIGIT$^-$PD-1$^+$, TIGIT$^+$PD-1$^+$, TIGIT$^+$PD-1$^-$) were present at higher frequencies in SF (Fig. 4I).

Mirroring CD4$^+$ T cells, CD8$^+$ T cells displayed a significantly higher expression of CD69 and CD103 in SF compared to PB (Fig. 4J) and CD8$^+$ T cells with a TIGIT$^+$PD-1$^+$ and TIGIT$^-$PD-1$^+$ phenotypes expressed the highest levels of both CD69 and CD103 (Fig. 4K and L).

To evaluate the effector function of the identified CD8$^+$ T-cells subset, we analyzed cytokine production both via scRNA-seq and by flow cytometry. In analogy to CD4$^+$ T lymphocytes, also for CD8$^+$ T cells (Fig. 5A and B) pseudotime representation of cytokine expression and dot plot showed that *IFNG and TNF* were mainly expressed by SF terminal clusters CD8-Teff and Trm. These data were confirmed at protein level by flow cytometry. We observed a significantly higher production of IFN-γ, TNF-α, and GM-CSF in SF compared to PB (Fig. 5C). IL-2, IL-17, and IL-10 were instead comparable between the two tissues.

Focusing on the four subsets identified based on TIGIT and PD-1 expression (Fig. 5D–I), all the analyzed cytokines were produced at higher levels by SF subsets than in PB-derived cells, with the exception of IL-17 and IL-10, which were produced at comparable levels. Regarding SF CD8$^+$ T cells, IL-2, IFN-γ, TNF-α, and IL-10 production was higher in TIGIT$^-$PD-1$^+$ and TIGIT$^+$PD-1$^+$ subsets, followed by the TIGIT$^-$PD-1$^-$ and TIGIT$^+$PD-1$^-$ populations. The production of GM-CSF instead was higher in the TIGIT$^-$PD-1$^-$ and TIGIT$^-$PD-1$^+$ subsets. Among PB CD8$^+$ T-cell subsets, no differences in cytokine production were observed, with the exception of the TIGIT$^-$PD-1$^-$ population, which produced the lowest percentage of all analyzed cytokines.

Characterization of synovial CD8$^+$ T cells' clonal expansion by TCR repertoire analysis

To gain insight into CD8$^+$ T cells clonality, we investigated their full-length TCR sequence from scRNA-seq data. As for CD4$^+$ T cells, the majority of clonotypes were private singletons (Supporting Information Fig. S6A), however, we observed a high degree of clonal expansion in both CD8$^+$ PB and SF cells (Fig. 6A). This finding agrees with data showing that CD8$^+$ T cells are generally more expanded than CD4$^+$ cells [18]. Interestingly, among the eight identified clusters, PB cluster Teff-GNLY$^+$ and SF cluster CD8-Teff showed the highest proportion of clonally expanded cells (Fig. 6B) and the lowest alpha diversity (Supporting Information Fig. S6). This observation is supported also by the trajectory analysis, which shows an enrichment of expanded clones at the end of branches 2 and 3, which terminate on clusters Teff-GNLY$^+$ and CD8-Teff, respectively (Fig. 6C–G). Also in CD8$^+$ T cells, we observed that many expanded clones were shared between clusters, such as clones 910 and 2660 (shared by cluster CD8-Teff and IFN stimulated) or 14 (shared by PB cluster Teff-GNLY$^+$ and SF cluster CD8-TIGIT$^+$) (Fig. 6H). This analysis revealed overlapping

clones from PB and SF, suggesting that CD8$^+$ T cells that locally expanded at sites of inflammation recirculate in the periphery.

Discussion

T-cell activity is finely regulated by IC molecules that provide stimulatory or inhibitory signals. Inhibitory ICs are commonly upregulated following T-cell activation and in the course of chronic inflammation to constrain T-cell responses and avoid tissue damage. Providing an inhibitory signal or blocking a stimulatory signal to achieve immune suppression is desirable for treating autoimmune diseases [19]. In keeping with this, abatacept, a humanized fusion protein targeting the CTLA-4 axis, approved for rheumatoid arthritis and polyarticular JIA treatment, can improve symptoms and reduce inflammation by suppressing T-cell responses [20–22]. However, an in-depth characterization of the role of IC expression by T cells in rheumatic diseases and, in particular, in JIA is still missing. In this study, we investigated at single-cell level the feature of T cells in JIA chronic inflammation both at sites of active inflammation.

Our results showed a prevalence of effector memory T cells in SF, which were antigen experienced and chronically reactivated, as suggested by the increased expression of ICs [23–25].

Dissecting the composition of CD4$^+$ T cells, we observed a heterogeneous pattern of gene expression in SF clusters due to different expression levels of Trm markers, effector genes, and ICs. Despite this high heterogeneity, based on trajectory analysis, we could identify two main SF T-cell lineage. Both SF trajectory branches showed high expression of genes typical of the Th1- and Th17- like phenotypes. This result is in accordance with other studies, which demonstrated the predominance of classical Th1, or nonclassical (Th17-derived) Th1 cells in the inflamed joints of children with JIA [26]. Moreover, the enrichment of IFN-γ–producing CD4$^+$ T cells in the SF has been associated with an extended disease course, suggesting that this population may drive severe disease [11, 12, 27]. Cells of both terminal branches exhibited characteristics of pathogenic cells in chronic inflammation. Cells of branch 2 showed the highest cytotoxic function despite the high expression of *PDCD1*. Interestingly, some cells of branch 2 terminal cluster Trm exhibited a Trm-like gene signature and expressed high levels of *TNF* and *IFNG*, indicating that they reside in the synovia and may support activation of myeloid cells involved in chronic inflammation [28]. Notably, Th1 cells, which produce high *IFNG* levels, have been already reported in JIA initiation and progression due to their high proinflammatory capability [13]. Terminal cluster Teff-TIGIT$^+$ instead was characterized by expression of both *TIGIT* and *PDCD1* and a lower cytotoxic capability. These results at the transcriptomic level highlight that CD4$^+$ T lymphocytes of JIA patients, once inside the inflamed joints, are prone to differentiate into cells with a high effector function despite the expression of inhibitory ICs, such as *TIGIT* and *PDCD1*, and to acquire a tissue-residency phenotype.

These findings were also confirmed at the protein level. In particular, flow cytometry data demonstrated that SF samples were
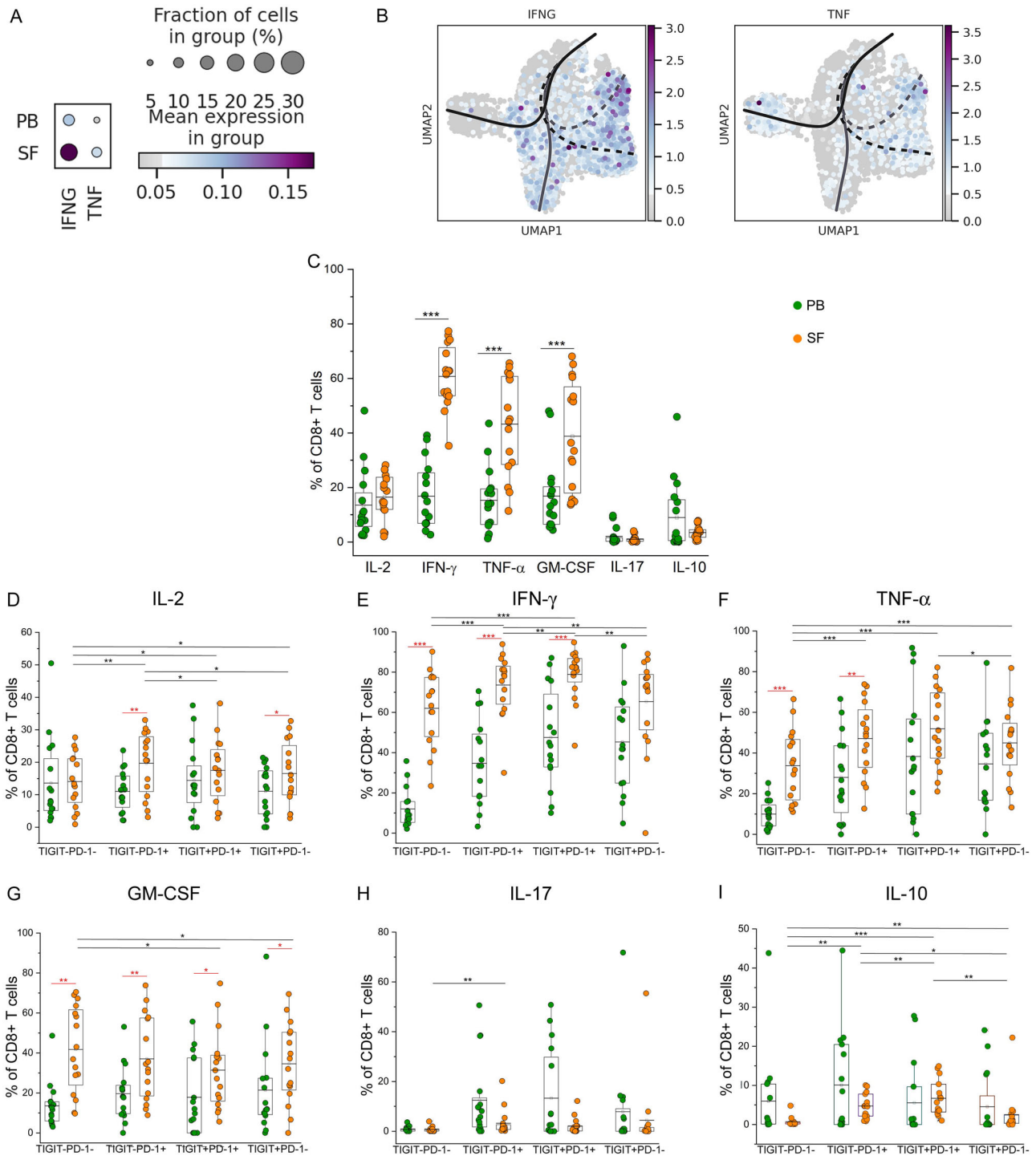
Figure 5. Functional characterization of PB and SF CD8$^+$ T-cell subsets expressing distinct combinations of inhibitory checkpoints. (A) Dot plot representation of scRNA-seq data showing the mean expression of cytokine genes in pooled CD8$^+$CD45RO$^+$ T cells from PB and SF of six patients. The size of the dot is proportional to the percentage of cells expressing the gene in that cluster, and the color code illustrates the average level of expression of all cells in the cluster. (B) UMAP visualization of CD8 cells colored by cytokines expression levels (C) Frequency of total CD8$^+$ T cells producing cytokines (IL-2, IFN-γ, TNF-α, GM-CSF, IL-17, IL-10). Frequency of CD8$^+$ T-cell subsets (TIGIT$^-$PD-1$^-$, TIGIT$^-$PD-1$^+$, TIGIT$^+$PD-1$^+$, TIGIT$^+$PD-1$^-$) producing IL-2 (D), IFN-γ (E), TNF-α (F), GM-CSF (G), IL-17 (H), IL-10 (I). (C-I) T cells were obtained from PB (green dots) (n = 16) and SF (orange dots) (n = 16) samples. Flow cytometric data (C-I) are obtained from 16 independent experiments. Boxes indicate mean values and 25th and 75th percentiles. Whiskers indicate minimum and maximum values. Statistical analysis was performed by Wilcoxon-Signed Rank test (*p < 0.05, **p < 0.01, ***p < 0.001). Red asterisks refer to paired statistics of PB compared to SF samples. Black asterisks represent paired statistics within each TIGIT and PD-1 subset in SF samples.
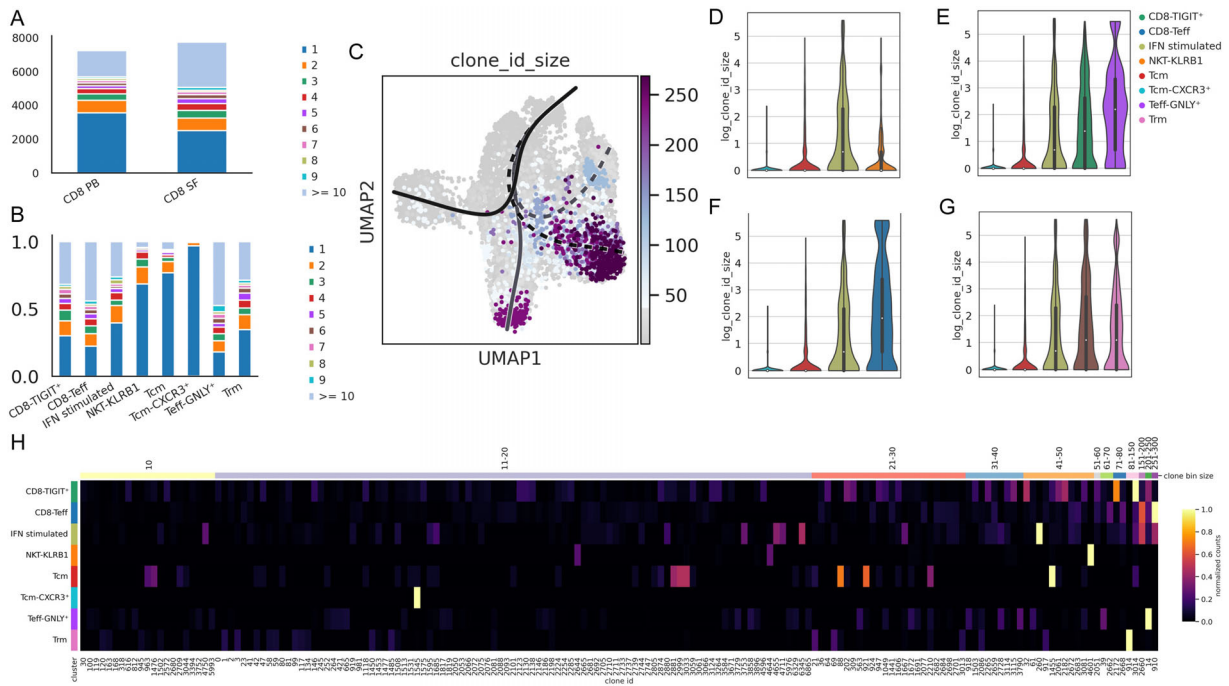
Figure 6. Single-cell TCR profiling of PB and SF CD8$^+$ T lymphocytes. Bar plots showing the clonal expansion of CD8$^+$ T cells from PB and SF of six patients (A) divided based on tissue origin or (B) divided in the identified clusters, each color represents the number of cells within the same TCR. (C) UMAP visualization of pseudotime trajectory together with clone size score in a logarithmic scale. Visualization of clone size as Violin plot in branch 1 (D), branch 2 (E), branch 3 (F), and branch 4 (G) clusters. (H) Heatmap showing the presence or absence of a specific clone in all identified cluster, the color code illustrates the relative abundance of each clone in the corresponding cluster. Clones are grouped by clone size and only clones with $\geq$ 5 cells were shown.

enriched in CD4$^+$ T cells with a TIGIT$^-$PD-1$^+$ and a TIGIT$^+$PD-1$^+$ phenotype. This observation indicates a prevalence of T cells expressing PD-1 in SF. Despite the fact that PD-1 is involved in the acquisition of an exhausted phenotype by T cells in cancer [29], it is a marker of activation and defines antigen-experienced T cells [30]. In agreement with this observation, high expression of ICs, such as PD-1, LAG3, and TIGIT, has already been observed on T cells obtained from the SF of patients with rheumatoid arthritis [31], raising the question whether these cells represent an effector rather than a functionally impaired cell subset. Our findings demonstrate that PD-1-expressing synovial infiltrating CD4$^+$ T lymphocytes are highly proinflammatory, as they express a significant amount of proinflammatory cytokines in vivo, following restimulation ex vivo.

Interestingly, studying the individual TCR α–β pairs of CD4$^+$ T cells, we found that cells of terminal cluster 3, expressing high levels of PDCD1 and producing proinflammatory cytokines, included the highest proportion of clonal cells, further suggesting their roles in sustaining chronic inflammation.

We used the same approach to dissect the diversity of CD8$^+$ T cells. Most CD8$^+$ cells derived from both tissues, PB and SF, expressed high levels of granzymes and other cytotoxic genes, according to their cytotoxic nature. Based on trajectory analysis, we could identify two SF terminal clusters (CD8-Teff and Trm), in particular, cluster Trm was characterized by cells showing a Tc1-like phenotype with expression of *CXCR3, STAT1, STAT2, TBX21,*

and *IFNG*. On the other hand, terminal cluster CD8-Teff resembled the high proinflammatory profile of synovial CD4$^+$ T cells, characterized by high expression of cytotoxic genes, *IFNG* and Trm markers together with IC molecules, such as *LAG3, TIGIT,* and *PDCD1*. Notably, most SF CD8$^+$ cells, in combination with ICs, expressed the transcription factor *TOX*, a marker associated with T-cell exhaustion in cancer [32, 33]. However, *TOX* expression has been associated also with a prolonged persistence of CD8$^+$ T cells during chronic viral infections and a promoted cytotoxic capacity in autoimmunity [34, 35]. Accordingly, our findings showed that *TOX*-expressing T cells retained their effector function and cytotoxic capability, corroborating the hypothesis that *TOX* expression in CD8$^+$ T cells is not exclusively linked with exhaustion, and in chronic inflammation, it is associated with a highly polyfunctional memory CD8$^+$ T-cell subset.

Protein data by flow cytometry confirmed that most SF CD8$^+$ T cells have a TIGIT$^+$PD-1$^+$ phenotype, and PD-1$^+$ cells are those with the highest proinflammatory phenotype, secreting high levels of IFN-γ and TNF-α and showing the highest degree of clonal expansion. Collectively, these findings confirm the data observed on the CD4$^+$ T-cell compartment and support that PD-1-expressing T cells in SF are active, rather than suppressed, and likely involved in sustaining chronic inflammation.

Recently, alongside circulating T cells, which are essential for providing immune protection, Trm cells were found capable of providing a better immunity in situ [36]. Trm cells have been

detected in many solid tumors, and an increase of this population in the tumor infiltrate has been correlated with a better prognosis and greater efficacy of therapy with IC-inhibitors [37]. Trm cells are also suspected of contributing to chronic inflammatory conditions [38]. Specifically, $CD4^+$ and $CD8^+$ Trm populations are found to be enriched in inflammatory diseases such as inflammatory bowel diseases [39] and MS [40]. An increased presence of $CD8^+$ Trm cells has been previously found in JIA [41]. Here, we found that also $CD4^+$ T cells display features of tissue residency in JIA. Notably, the highest expression of Trm markers was observed on $CD4^+$ and $CD8^+$ T cells-expressing PD-1, thus, cells with a high proinflammatory potential.

Collectively, our data demonstrate that despite the heterogeneity in the composition of synovial $CD4^+$ and $CD8^+$ T cells, those characterized by PD-1 expression were clonally expanded and displayed the highest proinflammatory capacity. In the last few years, several research groups, including us, have focused their efforts on understanding which is the main T-helper cell subset involved in JIA pathogenesis. T cells infiltrating the synovial membrane in JIA predominantly consist of Th1-skewed cells, which were thought to have a central role in the pathogenesis of the disease until the identification of Th17 subset. Up to now, the respective role of Th17 and Th1 cells in the pathogenesis of JIA is still debated, but both cell subsets play significant roles [42, 43], perhaps with different contributions in different patients or in different phases of the disease. Our data support the concept that novel therapeutic strategies targeting PD-1 may be effective in the treatment of JIA. These therapies may include both depleting strategies as well as the use of biological drugs, such as PD-1L-fusion proteins, capable to deliver an inhibitory signal on PD-1-expressing T cells. With this approach, it may become possible to collectively identify and target overactive T cells without the need to define their cytokine profile. By this way, the same drug may be effective in patients with different disease activity, in which the T-cell populations sustaining the inflammation can be different. Additional studies in vivo are needed to fully elucidate this.

Materials and methods

Patients

The study cohort includes 22 children with JIA recruited at the Pediatric Rheumatology Unit, Meyer Children Hospital, Florence, Italy. The diagnosis was made in accordance with the International League of Associations for Rheumatology classification criteria for JIA [44]. From each patient we obtained, at the time of active disease, PB and SF, the latter were obtained during knee therapeutic arthrocentesis. Demographic and clinical features of enrolled patients are summarized in Supporting Information Table S1. The procedures followed in the study were approved by local ethical committee on human experimentation.

PBMCs and SF mononuclear cells were obtained following density gradient centrifugation of samples using Lymphoprep (Axis Shield Poc As^{TM}).

Single-cell RNA-seq data processing

Raw unique molecular identifier counts for $CD4^+$ and $CD8^+$ cells from PB and SF of seven patients (GSE160097) were downloaded from Gene Expression Omnibus. Data processing (including normalization and identification of highly variable genes) and integration, and TCR analysis were performed with scanpy v1.9.1 [45] and scirpy v0.11.1 [46], respectively. A detailed description of scRNA-seq data processing is reported in Supporting Information (materials and methods section).

Immunophenotyping by flow cytometry

For lymphocyte cell subsets analysis by surface marker expression, PBMNC and SFMNC were washed in PBS + BSA (0.5%) and then stained for 15 min with fluorochrome-conjugated mAbs, using panels described in Supporting Information Table S2. Samples were acquired on a BD LSR II flow cytometer (BD Biosciences).

Intracellular cytokine production assay by flow cytometry

PBMNC and SFMNC were polyclonally stimulated for 5 h with PMA (10 ng/mL) and ionomycin (1 μM) for 5 h, the last three in the presence of Brefeldin A (5 μg/mL). Cells were then fixed in formaldehyde 2% (15 min at RT), washed in PBS + BSA (0.5%), and stained intracellularly with fluorochrome-conjugated mAbs using panels described in Supporting Information Table S3, in a buffer containing the permeabilizing agent saponin (0.5%). Samples were acquired on a BD LSR II flow cytometer (BD Biosciences). The gating strategy is shown in Supporting Information Fig. S7. All flow cytometric analyses were performed following published guidelines [47].

Statistical analysis

For analysis of the significance of differences between conditions or groups, the Mann-Whitney U test or the Wilcoxon test for paired samples was used. *p* values less than 0.05 were considered significant.

of Florence (ex-60%) derived from Ministero dell'Istruzione, dell'Università e della Ricerca (Italy) and partly funded by Novartis.

References

1 Ravelli, A. and Martini, A., Juvenile idiopathic arthritis. *Lancet*. 2007. **369**: 767–778.

2 Barut, K., Adrovic, A. and Şahin, S., Kasapçopur, Ö., Juvenile idiopathic arthritis. *Balkan Med J*. 2017. **34**: 90–101.

3 Cimaz, R., Marino, A. and Martini, A., How I treat juvenile idiopathic arthritis: a state of the art review. *Autoimmun. Rev.* 2017. **16**: 1008–1015.

4 Hinks, A., Cobb, J., Marion, M. C., Prahalad, S., Sudman, M., Bowes, J., Martin, P. et al., Dense genotyping of immune-related disease regions identifies 14 new susceptibility loci for juvenile idiopathic arthritis. *Nat. Genet.* 2013. **45**: 664–669.

5 McIntosh, L. A., Marion, M. C., Sudman, M., Comeau, M. E., Becker, M. L., Bohnsack, J. F., Fingerlin, T. E. et al., Genome-wide association meta-analysis reveals novel juvenile idiopathic arthritis susceptibility loci. *Arthritis Rheumatol.* 2017. **69**: 2222–2232.

6 Amariglio, N., Klein, A., Dagan, L., Lev, A., Padeh, S., Rechavi, G., Berkun, Y. et al., T-cell compartment in synovial fluid of pediatric patients with JIA correlates with disease phenotype. *J. Clin. Immunol.* 2011. **31**: 1021–1028.

7 Nüssing, S., Trapani, J. A. and Parish, I. A., Revisiting T cell tolerance as a checkpoint target for cancer immunotherapy. *Front. Immunol.* 2020. **11**: 589641.

8 Zhang, Q. and Vignali, D. A., Co-stimulatory and co-inhibitory pathways in autoimmunity. *Immunity* 2016. **44**: 1034–1051.

9 Mazzoni, A. and Cimaz, R., Targeting immune checkpoints in juvenile idiopathic arthritis: accumulating evidence. *Pediatr. Res.* 2021. **90**: 720–721.

10 Maschmeyer, P., Heinz, G. A., Skopnik, C. M., Lutter, L., Mazzoni, A., Heinrich, F., von Stuckrad, S. L. et al., Antigen-driven PD-1+ TOX+ BHLHE40+ and PD-1+ TOX+ EOMES+ T lymphocytes regulate juvenile idiopathic arthritis in situ. *Eur. J. Immunol.* 2021. **51**: 915–929.

11 Julé, A. M., Hoyt, K. J., Wei, K., Gutierrez-Arcelus, M., Taylor, M. L., Ng, J., Lederer, J. A. et al., Th1 polarization defines the synovial fluid T cell compartment in oligoarticular juvenile idiopathic arthritis. *JCI Insight* 2021. **6**: e149185.

12 Maggi, L., Mazzoni, A., Cimaz, R., Liotta, F., Annunziato, F. and Cosmi, L., Th17 and Th1 lymphocytes in oligoarticular juvenile idiopathic arthritis. *Front. Immunol.* 2019. **10**: 450.

13 Mazzoni, A., Maggi, L., Siracusa, F., Ramazzotti, M., Rossi, M. C., Santarlasci, V., Montaini, G. et al., Eomes controls the development of Th17-derived (non-classic) Th1 cells during chronic inflammation. *Eur. J. Immunol.* 2019. **49**: 79–95.

14 Gruarin, P., Maglie, S., De Simone, M., Häringer, B., Vasco, C., Ranzani, V., Bosotti, R. et al., Eomesodermin controls a unique differentiation program in human IL-10 and IFN-γ coproducing regulatory T cells. *Eur. J. Immunol.* 2019. **49**: 96–111.

15 Fergusson, J. R., Smith, K. E., Fleming, V. M., Rajoriya, N., Newell, E. W., Simmons, R., Marchi, E. et al., CD161 defines a transcriptional and functional phenotype across distinct human T cell lineages. *Cell Rep.* 2014. **9**: 1075–1088.

16 Zhou, L., Adrianto, I., Wang, J., Wu, X., Datta, I. and Mi, Q. S., Single-cell RNA-Seq analysis uncovers distinct functional human NKT cell subpopulations in peripheral blood. *Front. Cell Dev. Biol.* 2020. **8**: 384. PMID: 32528956; PMCID: PMC7264113.

17 Sun, Y., Wu, L., Zhong, Y., Zhou, K., Hou, Y., Wang, Z., Zhang, Z. et al., Single-cell landscape of the ecosystem in early-relapse hepatocellular carcinoma. *Cell* 2021. **184**: 404–421.e16. Epub 2020 Dec 23. PMID: 33357445.

18 Qi, Q., Liu, Y., Cheng, Y., Glanville, J., Zhang, D., Lee, J. Y., Olshen, R. A. et al., Diversity and clonal selection in the human T-cell repertoire. *Proc. Natl. Acad. Sci. USA.* 2014. **111**: 13139–13144. Epub 2014 Aug 25. PMID: 25157137; PMCID: PMC4246948

19 Pardoll, D. M., The blockade of immune checkpoints in cancer immunotherapy. *Nat. Rev. Cancer*. 2012. **12**: 252–264.

20 Ruperto, N., Lovell, D. J., Quartier, P., Paz, E., Rubio-Pérez, N., Silva, C. A., Abud-Mendoza, C. et al., Abatacept in children with juvenile idiopathic arthritis: a randomised, double-blind, placebo-controlled withdrawal trial. *Lancet* 2008. **372**: 383–391.

21 Álvarez-Quiroga, C., Abud-Mendoza, C., Doníz-Padilla, L., Juárez-Reyes, A., Monsiváis-Urenda, A., Baranda, L. and González-Amaro, R., CTLA-4-Ig therapy diminishes the frequency but enhances the function of Treg cells in patients with rheumatoid arthritis. *J. Clin. Immunol.* 2011. **31**: 588–595.

22 Maggi, L., Cimaz, R., Capone, M., Santarlasci, V., Rossi, M. C., Mazzoni, A., Montaini, G. et al., Immunosuppressive activity of abatacept on circulating T helper lymphocytes from juvenile idiopathic arthritis patients. *Int. Arch. Allergy Immunol.* 2016. **171**: 45–53.

23 Ricciardi, S., Manfrini, N., Alfieri, R., Calamita, P., Crosti, M. C., Gallo, S., Müller, R. et al., The translational machinery of human CD4+ T cells is poised for activation and controls the switch from quiescence to metabolic remodeling. *Cell Metab.* 2018. **28**: 895–906.e5.

24 Curdy, N., Lanvin, O., Laurent, C., Fournié, J. J. and Franchini, D. M., Regulatory mechanisms of inhibitory immune checkpoint receptors expression. *Trends Cell Biol.* 2019. **29**: 777–790.

25 Bengsch, B., Johnson, A. L., Kurachi, M., Odorizzi, P. M., Pauken, K. E., Attanasio, J., Stelekati, E. et al., Bioenergetic insufficiencies due to metabolic alterations regulated by the inhibitory receptor PDCD1 are an early driver of CD8(+) T cell exhaustion. *Immunity* 2016. **45**: 358–373.

26 Mazzoni, A., Maggi, L., Liotta, F., Cosmi, L. and Annunziato, F., Biological and clinical significance of T helper 17 cell plasticity. *Immunology* 2019. **158**: 287–295

27 **Cosmi, L., Cimaz, R., Maggi, L., Santarlasci, V., Capone, M., Borriello, F., Frosali, F. et al.**, Evidence of the transient nature of the Th17 phenotype of CD4+CD161+ T cells in the synovial fluid of patients with juvenile idiopathic arthritis. *Arthritis Rheum.* 2011. **63**: 2504–2515.

28 **Jain, A., Irizarry-Caro, R. A., McDaniel, M. M., Chawla, A. S., Carroll, K. R., Overcast, G. R., Philip, N. H. et al.**, T cells instruct myeloid cells to produce inflammasome-independent IL-1β and cause autoimmunity. *Nat. Immunol.* 2020. **21**: 65–74.

29 **Kim, P. S. and Ahmed, R.**, Features of responding T cells in cancer and chronic infection. *Curr. Opin. Immunol.* 2010. **22**: 223–230.

30 **Pentcheva-Hoang, T., Chen, L., Pardoll, D. M. and Allison, J. P.**, Programmed death-1 concentration at the immunological synapse is determined by ligand affinity and availability. *Proc. Natl. Acad. Sci. USA.* 2007. **104**: 17765–17770.

31 **Cho, B. A., Sim, J. H., Park, J. A., Kim, H. W., Yoo, W. H., Lee, S. H., Lee, D. S. et al.**, Characterization of effector memory CD8+ T cells in the synovial fluid of rheumatoid arthritis. *J. Clin. Immunol.* 2012. **32**: 709–720.

32 **Wang, X., He, Q., Shen, H., Xia, A., Tian, W., Yu, W. and Sun, B.**, TOX promotes the exhaustion of antitumor CD8+ T cells by preventing PD1 degradation in hepatocellular carcinoma. *J. Hepatol.* 2019. **71**: 731–741.

33 **Scott, A. C., Dündar, F., Zumbo, P., Chandran, S. S., Klebanoff, C. A., Shakiba, M., Trivedi, P. et al.**, TOX is a critical regulator of tumour-specific T cell differentiation. *Nature* 2019. **571**: 270–274.

34 **Yao, C., Sun, H. W., Lacey, N. E., Ji, Y., Moseman, E. A., Shih, H. Y., Heuston, E. F. et al.**, Single-cell RNA-seq reveals TOX as a key regulator of CD8+ T cell persistence in chronic infection. *Nat. Immunol.* 2019. **20**: 890–901.

35 **Page, N., Klimek, B., De Roo, M., Steinbach, K., Soldati, H., Lemeille, S., Wagner, I. et al.**, Expression of the DNA-binding factor TOX promotes the encephalitogenic potential of microbe-induced autoreactive CD8+ T cells. *Immunity* 2018. **48**: 937–950.e8.

36 **Gebhardt, T., Palendira, U., Tscharke, D. C. and Bedoui, S.**, Tissue-resident memory T cells in tissue homeostasis, persistent infection, and cancer surveillance. *Immunol. Rev.* 2018. **283**: 54–76.

37 **Amsen, D., van Gisbergen, K., Hombrink, P. and van Lier, R. A. W.**, Tissue-resident memory T cells at the center of immunity to solid tumors. *Nat. Immunol.* 2018. **19**: 538–546.

38 **Samat, A. A. K., van der Geest, J., Vastert, S. J., van Loosdregt, J. and van Wijk, F.**, Tissue-resident memory T cells in chronic inflammation-local cells with systemic effects? *Cells* 2021. **10**: 409.

39 **Zundler, S., Becker, E., Spocinska, M., Slawik, M., Parga-Vidal, L., Stark, R., Wiendl, M. et al.**, Hobit- and Blimp-1-driven CD4+ tissue-resident memory T cells control chronic intestinal inflammation. *Nat. Immunol.* 2019. **20**: 514.

40 **Machado-Santos, J., Saji, E., Tröscher, A. R., Paunovic, M., Liblau, R., Gabriely, G., Bien, C. G. et al.**, The compartmentalized inflammatory response in the multiple sclerosis brain is composed of tissue-resident CD8+ T lymphocytes and B cells. *Brain* 2018. **141**: 2066–2082.

41 **Petrelli, A., Mijnheer, G., Hoytema van Konijnenburg, D. P., van der Wal, M. M., Giovannone, B., Mocholi, E., Vazirpanah, N. et al.**, PD-1+CD8+ T cells are clonally expanding effectors in human chronic inflammation. *J. Clin. Invest.* 2018. **128**: 4669–4681.

42 **Maggi, L., Margheri, F., Luciani, C., Capone, M., Rossi, M. C., Chillà, A., Santarlasci, V. et al.**, Th1-induced CD106 expression mediates leukocytes adhesion on synovial fibroblasts from juvenile idiopathic arthritis patients. *PLoS One* 2016. **11**: e0154422.

43 **Margheri, F., Maggi, L., Biagioni, A., Chillà, A., Laurenzana, A., Bianchini, F., Bani, D. et al.**, Th17 lymphocyte-dependent degradation of joint cartilage by synovial fibroblasts in a humanized mouse model of arthritis and reversal by secukinumab. *Eur. J. Immunol.* 2021. **51**: 220–230.

44 **Petty, R. E., Southwood, T. R., Baum, J., Bhettay, E., Glass, D. N., Manners, P., Maldonado-Cocco, J. et al.**, Revision of the proposed classification criteria for juvenile idiopathic arthritis: Durban, 1997. *J. Rheumatol.* 1998. **25**: 1991–1994. PMID: 9779856.

45 **Wolf, F., Angerer, P. and Theis, F.**, SCANPY: large-scale single-cell gene expression data analysis. *Genome Biol.* 2018. **19**. https://doi.org/10.1186/s13059-017-1382-0.

46 **Sturm, G., Szabo, T., Fotakis, G., Haider, M., Rieder, D., Trajanoski, Z. and Finotello, F.**, Scirpy: a Scanpy extension for analyzing single-cell T-cell receptor-sequencing data. *Bioinformatics* 2020. **36**: 4817–4818. PMID: 32614448; PMCID: PMC7751015.

47 **Cossarizza, A., Chang, H. D., Radbruch, A., Acs, A., Adam, D., Adam-Klages, S., Agace, W. W. et al.**, Guidelines for the use of flow cytometry and cell sorting in immunological studies (second edition). *Eur. J. Immunol.* 2019. **49**: 1457–1973.

Abbreviations: **JIA**: juvenile idiopathic arthritis · **IC**: immune checkpoint · **scRNA-seq**: single-cell RNA-sequencing · **PB**: peripheral blood · **SF**: synovial fluid · **Tcm**: T-central memory · **Trm**: tissue-resident memory cell · **UMAP**: Uniform Manifold Approximation and Projection

Full correspondence: Dr. Laura Maggi and Prof. Francesco Annunziato, Department of Experimental and Clinical Medicine, University of Florence, Viale Pieraccini, 6, 50134-Firenze, Italy
e-mail: laura.maggi@unifi.it; francesco.annunziato@unifi.it